ELSEVIER

Ore Geology Reviews 13 (1998) 381–406

ORE GEOLOGY REVIEWS

Wallrock alteration in the Bendigo gold ore field, Victoria, Australia: Uses in exploration

X. Li *, T.A.P. Kwak, R.W. Brown

School of Earth Sciences, La Trobe University, Bundoora, Vic. 3083, Australia

Received 16 April 1997

Abstract

The Bendigo goldfield, which has produced most of Victoria's gold (22 million ounces = 684.3 ton), consists of numerous deposits located mainly along narrow, parallel-trending anticlinal domes separated by 100 to 400 m. The individual domes are parts of a regional anticlinorium in Lower Ordovician sedimentary rocks. Highest gold ore values are generally located in the eastern limbs and particularly in the apical areas of the smaller individual anticlinal domes and in the central part of the more regional-anticlinorium.

Alteration present in metasandstone units in the Nell Gwynne anticline consists of phengitic sericite (to 15 vol%), chlorite (to 7%), carbonates (siderite, sideroplesite, ankerite and calcite, to 10%) and sulphides (arsenopyrite, pyrite, chalcopyrite and sphalerite, to 5%). The alteration generally follows the trend of the structure extending upward and above mineralisation in anticlinal areas and below largely unmineralised synclinal areas. Phengitic sericite extends furthest, to at least 150 m above mineralised saddle reef positions, chlorite to 130 m, sulphides to 80 m and carbonate to 50 m. Chlorite geothermometry suggests temperatures of 260 to 290°C for the alteration. The sequence of carbonate precipitation generally is from siderite (early), sideroplesite, ankerite and calcite. The more Fe-rich carbonates tend to occur near the apical parts of the anticlinal domes. Arsenopyrite occurs within 10 m of the veins, while hydrothermal pyrite, chalcopyrite and sphalerite all extend to 50 m. Framboidal pyrite (possibly greigite) present in unaltered metasediments becomes progressively recrystallised and replaced by hydrothermal pyrite, chalcopyrite and sphalerite as mineralisation is approached. Hydrothermal pyrite is generally euhedral and anomalous in having high As contents when compared to framboidal pyrite.

Maximum Au grades (205 ppm) occur in the saddle reef position and below a thick shale unit. Lower-grade mineralisation (0.5–6.0 ppm) occurs above this in the overlying stratigraphy. As and Pb anomalies cross cut the alteration zoning and occur as plume-like dispersion haloes above the mineralisation. The Au occurs in and near the As 'plume'. Cu concentrations reach their maximum values adjacent to high Au values. Measured CO_2 values confirm the observed carbonate distributions. H_2O^+ and Zn values in the section show relatively random distributions.

Two separate stages of mineralisation are indicated, the earlier localised within classic saddle reef structures and containing the highest Au, Cu and some As and a later, cross-cutting stage of mineralisation associated with high As. The alteration is mainly associated with the former.

Keywords: lode-gold mineralisation; wallrock alteration; Bendigo goldfield; Victoria; Australia

* Corresponding author.

0169-1368/98/$19.00
PII S0169-1368(97)00027-9

1. Introduction

The nature and extent of the alteration of wall rocks marginal to mesothermal gold vein deposits is important for understanding the genesis of gold-vein deposits and can be used as a guide for exploration. Such alteration has been studied by a large number of authors (e.g. Kuhns, 1986; Ames et al., 1991; Love and Roberts, 1991; Sketchley and Sinclair, 1991; McCuiag and Kerrich, 1994) who have found that altered wall rocks are typically enriched in precious metals (Au, Ag), associated rare elements (As, Sb, Se, Te, Bi, W, B), LILE (K, Rb, Ba, Li, Cs, Tl) and volatiles (H_2O, CO_2, CH_4, H_2S). The mineralogy of wall rock alteration depends upon the nature of the precursor, physiochemical conditions of the ore fluids and the temperature and pressure of the environment. Different deposits formed at significantly different temperatures within similar lithologies may be associated with distinctly different styles of alteration (Mueller and Groves, 1991; Groves et al., 1992). In the sub- to mid-greenschist facies environment the minerals typically found in psammitic rocks are albite, muscovite/phengite, chlorite, carbonates (ankerite, dolomite), sulphides and less commonly biotite and tourmaline (e.g. McCuiag and Kerrich, 1994).

Most of the existing studies document alteration of mafic, ultramafic, granitoid and BIF-hosted mineralisation common in Precambrian terranes. Palaeozoic turbidite-hosted Au-vein mineralisation has not received the same degree of study. A number of workers have reported on very similar styles of mineralisation to those found in Victoria occurring in Nova Scotia, Canada, including saddle reef-style mineralisation (Kontak et al., 1990). In Nova Scotia, two styles of alteration are recognised. An early period of pervasive silicification, localised sulphide alteration and minor phyllic alteration is widespread (e.g. 5 km along strike and 1 km across strike of a deposit). More localised, less intense, alterations consisting of 10 cm wide orange–beige alteration haloes surround calcite–chlorite veinlets. Similar geochemical studies on mineralisation-related alteration in central Victoria has received little attention apart from published studies by Bowen (1972), Stock and Zaki (1972), Stüwe et al. (1988) and Cox et al. (1991, 1995). These studies indicate that there are As (arsenopyrite), S (sulphides), CO_2 (carbonates) and Au additions to the wall rocks in the Eureka and Wattle Gully mine of the Castlemaine goldfield in central Victoria and Sb addition at the Costerfield deposits.

Central Victoria, Australia, constitutes one of the ten major primary gold regions of the world (Phillips and Powell, 1992) and one of the few such regions present in Palaeozoic rather than Precambrian terrains. The Bendigo ore field, Australia's second largest goldfield, is located in central Victoria, 152 km NNW of Melbourne and covers an area of 45 km^2. It produced approximately 22 million ounces of gold, 17 million ounces from reef mining, which is approximately 53% of the primary gold produced in Victoria. Mineralisation is mainly restricted to narrow, structurally controlled fault- and fold-related dilatant zones and wider, disseminated and veinlet-hosted mineralisation within a Lower Ordovician turbidite sequence. The nature of mineralisation at Bendigo has been documented by many authors during mining activity (e.g. Dunn, 1896), who have given some insights into the geology of the field. More modern approaches have been facilitated by recent work by the Western Mining Corp. and Bendigo Mining N.L. who have provided access to the Deborah anticline for underground mapping, observing and sampling, as well as abundant drill core material from the Nell Gwynne anticline.

The present study is mainly concerned with the extent and nature of wall rock alteration, its distribution and that of pathfinder elements, such as As, and how these relate to the characteristics of the mineralisation and fluid flow paths.

2. General features of the Bendigo ore field

The ore field is hosted by the Lower to Middle Ordovician Castlemaine Supergroup (Cas and VandenBerg, 1988) in turbidite sedimentary rocks, 2–3 km west of the major Whitelaw fault and 10 km NNE of the Middle Devonian Harcourt Batholith (Fig. 1). The host rocks are typical turbidites, exhibiting characteristic Bouma cycles (Bouma, 1962). Sandstones, siltstones and shale (some of which are graphitic) also occur. There are thin polymict con-

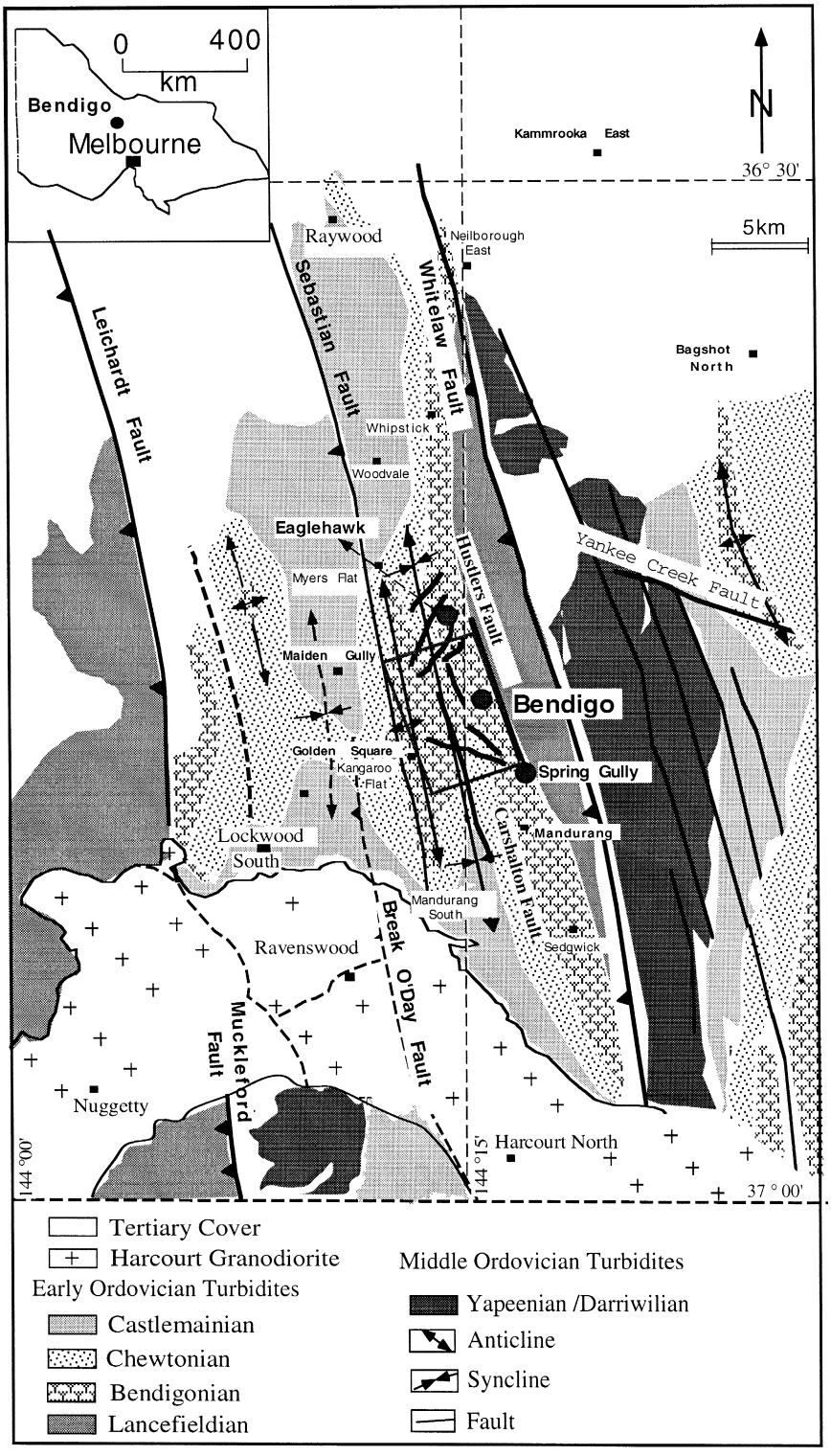

Fig. 1. The location of the Bendigo goldfield (after Sharpe and MacGeehan, 1990).

glomerates and rare cone-in-cone (Wilkinson, 1988; Willman and Wilkinson, 1992) limestone units up to 20 cm in thickness. The latter grade into siltstone, are continuous for hundreds of meters and consist of pure ankerite (Willman and Wilkinson, 1992). Upward fining of turbidite packages, as found at Bendigo (Sharpe and MacGeehan, 1990), are typical of deep sea submarine fan deposition (e.g. Cas, 1983).

On a regional scale, the host rocks have been folded into NNW-trending anticlinoria and synclinoria with a reversal of plunge roughly coinciding to an E–W axis bisecting the ore field (Sharpe and MacGeehan, 1990). The central 'goldfield structural domain' (Willman and Wilkinson, 1992) is bounded to the east by the Lightning Hill anticline, east of which is the 'eastern structural domain' and to the west by the Kangaroo anticline. The Whitelaw fault is considered to be the lower bounding fault of one thrust sheet, with the 'goldfield domain' being the core of the thrust slice and the 'eastern structural domain' forming its base. In the 'goldfield structural domain' individual folds within the major structures are chevron to accordion style with interlimb angles of 40–50°, amplitudes of 100 to 300 m and axial planes dipping 75–85°E. The doubly plunging nature of these folds yields domal structures. In the 'eastern structural domain' the folds are tighter with interlimb angles of 30°, the host rocks have a slightly higher metamorphic grade (phyllites as opposed to shales in the goldfields structural domain) and little gold mineralisation occurs (Willman and Wilkinson, 1992).

The sequence has been metamorphosed to lower-middle greenschist facies resulting in the formation of metamorphic sericite and very minor chlorite, defining a poorly developed foliation (S_1), as well as the recrystallisation of quartz. Detrital plagioclase and muscovite remained largely unaffected. Bedding (S_0) and the poorly defined metamorphic foliation (S_1) were folded into tight, often chevron type, folds with an axial plane cleavage (S_2). In places bedding and ore-bearing veinlets are offset by this surface. It is possible that the development of S_2 followed S_1 in a continuous process as folding became progressively tightened.

Mineralisation occurs as classic concordant saddle reefs. However, much of the ore occurs in discordant veins, particularly in the apical areas of domes (e.g. Deborah fault and 'back'). Mineralisation pre-, syn- and post-dated folding. Folded, mineralised laminated veins are intersected by mineralised 'spur' and other veins which show varying degrees of folding. Carbonate alteration 'spots' related to mineralisation have been attenuated along fold limbs and mineralised veinlets are displaced by the axial plane cleavage (S_2).

At least 15 major anticlinal domes exist in the 'goldfield structural domain' containing mineralisation of variable gold grades and tonnages. Average historic production grades were 10 to 15 g/tonne. The mineralisation includes saddle reef style veins and shear-hosted veins but also sandstone-hosted mineralisation, some of which occurs in synclinal rather than anticlinal positions (Kwak and Roberts, 1996). The greater part of past production came from veins in parallel-trending anticlines; the Garden Gully, Hustlers and New Chum anticlinal domes. Significant production also came from 9 others including the Nell Gwynne and Deborah anticlinal domes.

3. Study and analytical methods

Detailed alteration studies on host rocks such as Palaeozoic turbidite sequences are not common, partly because of the difficulty of establishing whether bulk compositional differences between supposedly altered rocks and unaltered rocks are due to alteration or due to sedimentary facies differences. In addition, minerals such as chlorite, sericite, carbonate and sulphides, found as alteration peripheral to many mesothermal gold vein deposits in psammitic and pelitic turbidite host rocks, are very similar to those produced by regional or contact metamorphism, or those of detrital origin. Care was taken here to differentiate between these possible origins on the basis of textural and compositional differences.

Ideally, mineral and elemental distributions should be studied in 3 dimensions, but the volume of work involved would make such a study too difficult and there is seldom enough suitable study material available. The area chosen for detailed study, the Nell Gwynne anticline near the Spring Gully reservoir

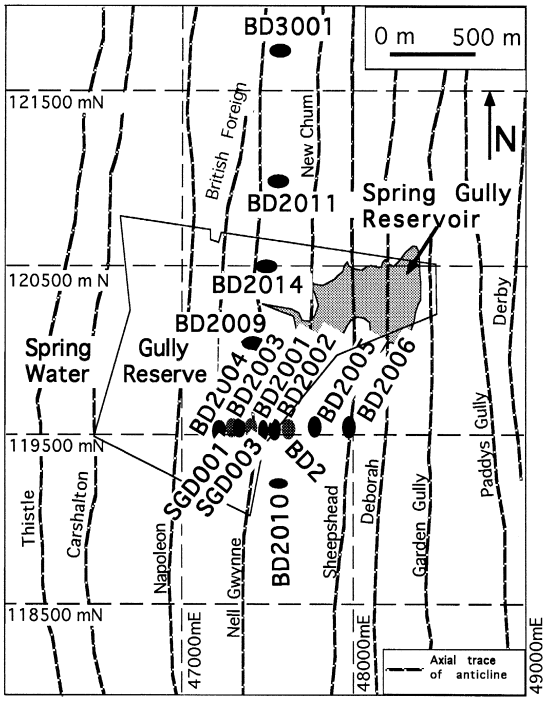

Fig. 2. Plan view of the Nell Gwynne anticlinal dome showing the positions of drill holes used in this study and other anticlinal zones.

(Fig. 2), is characterised by typical Bendigo ore field geology. This area was chosen because of the availability of extensive diamond drill core from 14 drill holes across the anticline (119500N sect(Fig. 2). Drill core coverage extended from well outside the mineralised area, in the adjacent syncline, across the anticline into the next syncline. In addition, numerous diamond and percussion drill holes along the axis of the anticline were available. Thus both cross- as well as long-section samples were studied.

The previous operating company at Bendigo (Western Mining Corp.) undertook chemical analyses of available drill core material, resulting in many thousands of analyses for As, Au, Pb, Cu and Zn and some for Hg and provided access to these for this study. Samples were analysed by standard commercial procedures, mainly atomic absorption and fire assay (for gold). The CO_2 and H_2O data for this study were analysed at La Trobe University from the approximately 41 samples shown in Fig. 3. H_2O^- was determined by gravimetry and H_2O^+ and CO_2 by furnace infrared spectrometry using a LECO-RC-412 analyser, respectively. The geochemical and CO_2–H_2O^+ data presented in cross section was contoured using a commercial contouring program (MacGRIDzo).

4. Hydrothermal alteration in the Nell Gwynne anticline

4.1. 119500N cross section

Fig. 2 shows a plan view of the Nell Gwynne anticline and Fig. 3 the 119500 section across the anticline. The section contains an anticlinal and part of a synclinal structure defined by alternating beds of sandstone, carbonaceous sandstone, siltstone, silty shale and shale. Quartz veins occur mainly in the core of the anticline, where most exhibit varying degrees of brittle deformation and dynamic crystallisation. It is noteworthy that most of the veining in the core of the anticline terminates near the lower contact of the lowermost and thickest black shale/slate unit in the section. The importance of this will be discussed. Ten drill holes intersected the anticline and approximately 70 core samples were analysed.

Fig. 4 A shows the distribution of vein quartz (I) and pod-like quartz, which includes the sheared and deformed quartz occurring near the core of the anticline and syncline on section 119500N (II). Sheared quartz is typically clear to grey where it is gold bearing and the Au is intimately associated with carbonates and sulphides within white ‘bull’ quartz. In the thin section the quartz shows undulatory extinction, some recrystallisation as well as cataclasis. In some places clear quartz occurs as a fine-grained breccia, 1–2 cm thick, within massive veins.

Carbonate occurs both in quartz veins and wall rocks. Its abundance in the latter decreases from near the core of the anticline outwards. Nearest the massive veins, in the core of the anticline, more than 5 vol% carbonate occurs decreasing to 0% between 50 and 130 m outward from the core (Fig. 4B). Carbonate occurs as: interstitial grains between quartz grains (Fig. 5A), as ovoid ‘spots’ (Fig. 5B), as subhedral rhombs (Fig. 5C) and in carbonate veins (Fig. 5C).

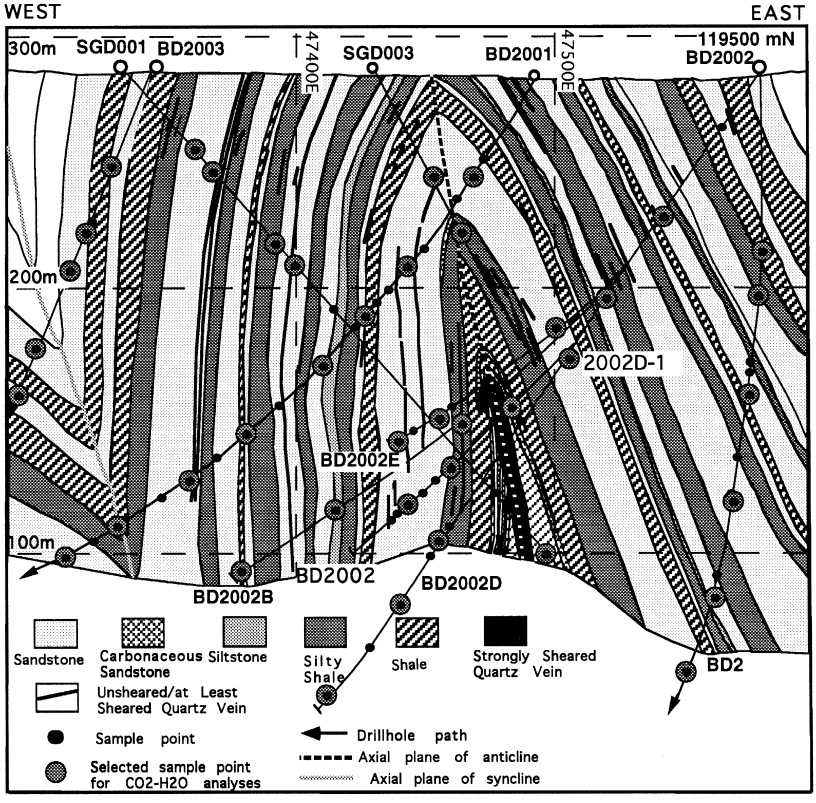

Fig. 3. The 119500N cross section of the Nell Gwynne anticlinal dome showing the positions of samples, drill holes and the general geology (approximately 70 samples shown).

The compositions include siderite, sideroplesite, ankerite and calcite (Table 1) and Fig. 6). Generally there appears to be a progressive change from Fe-rich to Fe-poor compositions. The sideroplesite occurs around the siderite spots and both of them were truncated by the S_2 cleavage. However, in the same thin section ankerite (high-Mn) spots were not offset by S_2. According to the mineral relationships as shown in Fig. 5C, it is noteworthy that different ankerite (low-Mn) compositions occur around calcite rhombs and veinlets (I) which belong to the early stage hydrothermal alteration products. Therefore the order of mineral formation is siderite → sideroplesite → ankerite (high-Mn) → calcite in the early alteration stage (Fig. 6). The late alteration stage consists of the low-Mn ankerite and calcite both of which occur as interstitial/crustiform(rim)-shaped (II in Fig. 5C)/small veinlet-shaped carbonate. Thus carbonate formed after metamorphism (S_1) and both before and after cleavage (S_2) associated with folding. No sedimentary layers of carbonate were found in the sequence.

Sericite also occurs in both the mineralised veins and wall rocks. However, in the latter, it is difficult to distinguish from detrital muscovite and metamorphic sericite. Detrital muscovite (sericite) is generally oriented parallel to bedding and occurs as larger grains (Fig. 7A). In Fig. 7A metamorphic sericite can be seen to define a foliation oriented at an acute angle to the long axis of the detrital muscovite. The latter grains have a lower phengitic component (Fig. 8A). Metamorphic sericite also appears to have been folded while hydrothermal sericite often cross cuts most features (Fig. 7B and C). Metamorphic sericite tends to be less phengitic than hydrothermal sericite but some overlap exists (Table 2, Fig. 8A). The distribution of hydrothermal sericite varies from 10 vol%, nearest the core of the anticline, to 0% at least

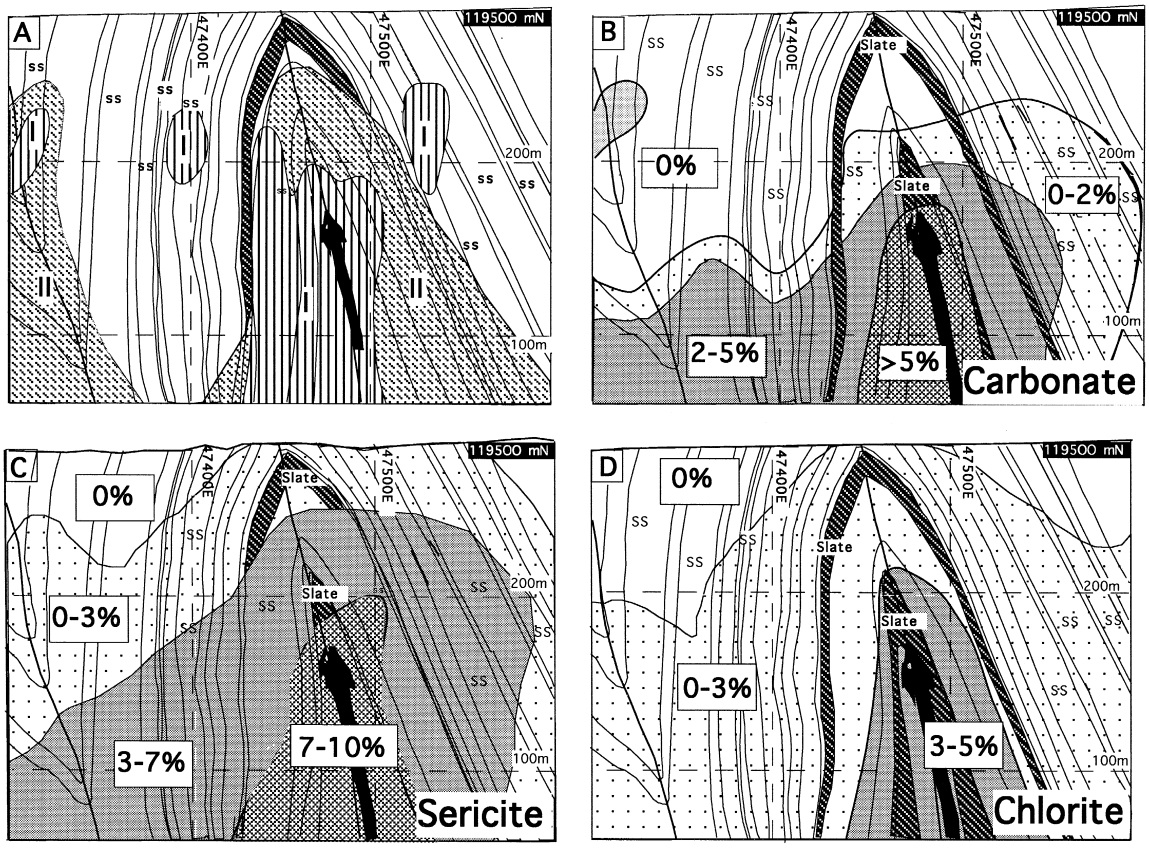

Fig. 4. The distribution of quartz veins and sheared quartz, carbonate, sericite and chlorite in the 119500N cross section. (A) Distribution of quartz veins (I) and pod-like quartz, which includes the sheared quartz occurring near the core of the anticline and syncline (II). (B) Carbonate distribution. (C) Sericite distribution. (D) Chlorite distribution.

150 m both above and lateral to the core (Fig. 4C). Sericite generally predates S_2 but again, in many cases, no clear relationship could be established.

Chlorite occurs mainly in the wall rocks and rarely in some of the gold bearing veins (called 'the irish' by early miners). The compositions include ripidolite and pycnochlorite. They are considered as the early stage alteration and the later stage alteration minerals, respectively (Table 3, Fig. 8B). Chlorite occurs both as discrete grains, often associated with hydrothermal sericite/carbonate and as a replacement of detrital muscovite (Fig. 5A, 7D). It reaches abundances as high as 5 vol% in the anticline's core, but falls to 0 vol% approximately 100 m away from the core (Fig. 4D).

The sulphides arsenopyrite, chalcopyrite, sphalerite and pyrite occur from the core of the anticline to 90–140 m away (Fig. 9A). Arsenopyrite occurs as euhedral grains nearest the core of the anticline as well as up to at least 100 m above the core. Hydrothermal pyrite (as cubes), chalcopyrite and sphalerite occur in a zone up to 110 m from the core of the anticline while framboidal pyrite occurs beyond this. The framboidal pyrite is believed to be sedimentary in origin, having formed just below the sediment–sea water interface and its origin possibly involved bacterial activity (Sweeney and Kaplan, 1973; Fenchel and Blackburn, 1979). Nearest the core of the anticline, spheroids contain crystalline, subhedral pyrite, chalcopyrite and sphalerite (Fig. 10 A, B and C). Further out there are framboidal bodies containing individual spheroids showing an internal cell-like texture (Fig. 10D). Gold has been detected in these textures. Probe data show that gold contents

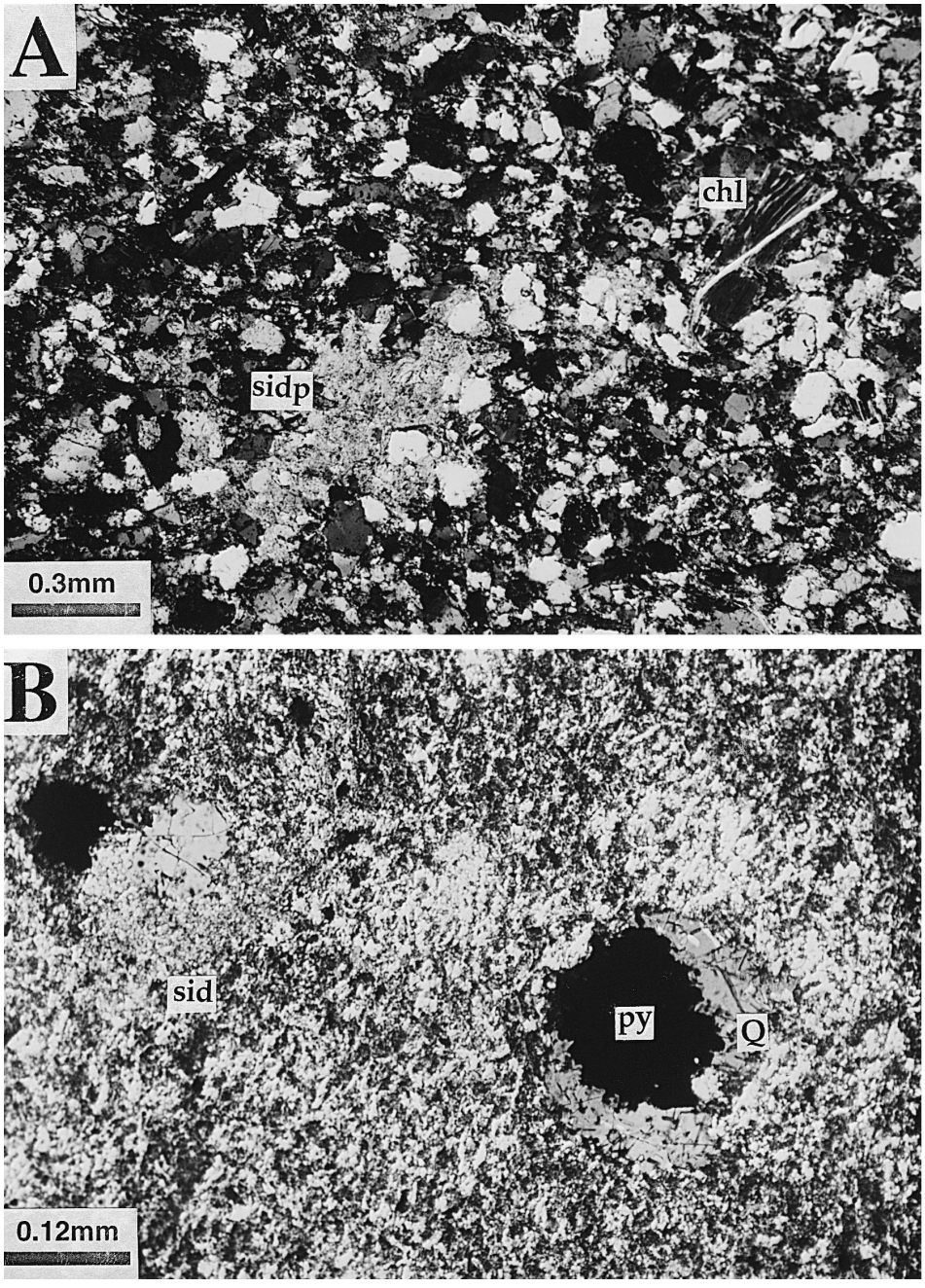

Fig. 5. Photomicrographs of textures of carbonate minerals. (A) Interstitial carbonate: the sideroplesite (sidp) occurs between quartz grains but appears to have replaced other constituents of the rock including detrital plagioclase, micas and metamorphic sericite. (B) Ovoid carbonate spots: the siderite (sid) spots occur as rounded bodies in this case with pyrite (py) and quartz (Q). They only include minor quantities of original detrital mineral material. (C) Rhombs of carbonate and carbonate in veins: the rhombs consist of an inner core of calcite (cal, I) and an outer rim of ankerite (ank, II) while the vein contains ankerite (II) along its margins and a core of calcite (I) in its core. The conflicting information may indicate multiple mineralising events.

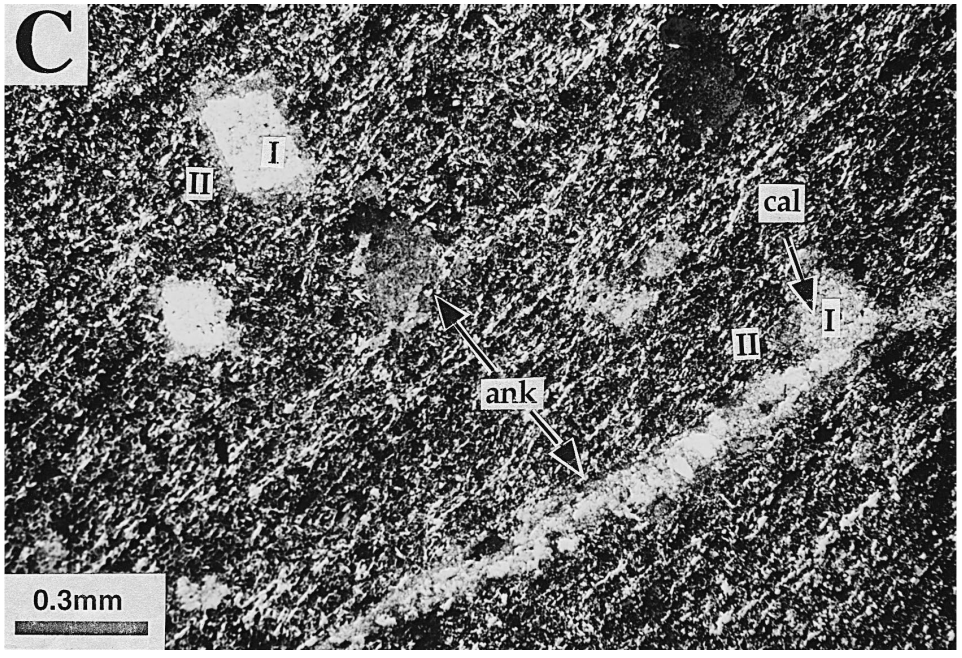

Fig. 5 (continued).

range from 0 to 1150 ppm (detection limit: 100 ppm) in frambiodal sulphides.

4.2. Long section of the Nell Gwynne anticline

The general geology of the Nell Gwynne anticline and the variation of carbonate varieties, chlorite occurrences and formation temperatures and the proportion of phengite, as determined by the Si:Al(IV) ratio present in hydrothermal sericite–phengite are shown in Fig. 11. The distribution of the most intense alteration suggests that the apex of the anticlinal dome is located between the 121000N and 120500N sections (Fig. 11A). In this vicinity many samples contain up to 50% carbonate and greater than 10% chlorite and sericite.

The distribution of carbonate in terms of textural types and compositional variations along the Nell Gwynne anticline suggests that identifiable differences occur along this anticlinal dome (Fig. 11A). The 121750N section has only ankerite and calcite; the 120950N section, sideroplesite and ankerite; the 120500N section, sideroplesite, ankerite and siderite while the southernmost section, 119500N, has all four carbonates. The variety of carbonate compositions observed in the 119500N section may be an artefact, seeing that more analyses were done in this area compared with the other sections studied. Alternatively, they may reflect different phases of carbonate precipitation associated with multi-stage fluid flow within the Bendigo goldfield. The greatest proportion of Fe-rich carbonate occurs in the 120950N and 120500N sections, which is consistent with the degree of alteration being more intense in this area.

Fig. 11B shows the distribution of hydrothermal phengitic sericite in the long section of the Nell Gwynne anticline. The hydrothermal sericite can be divided into two groups: (I) lower Si:Al (IV) ratio phengites (3.8–5.1) and (II) higher Si:Al (IV) ratio phengites (5.5–7.2). Group (I) hydrothermal phengitic sericites are associated with siderite/sideroplesite/ankerite (high-Mn), clear, sheared quartz (gold rich) and relatively higher temperature chlorite (main/early alteration stage). The Si:Al (IV) ratios vary from 3.8 to 5.1 with the average values in the long section being different (121750N, 4.34; 120950N, 4.36; 120500N, 4.58; 119500N, 7.28). Phengites with the highest average Si:Al (IV) ratio occur in the apex of the dome between the 120950N and 120500N sections. In contrast, group (II) phen-

Table 1
Representative analyses of two stage hydrothermal carbonates (I and II)

Sample No.	Locality (m)	Description	Mineral	Oxide (wt%)							Cations based on 6(O)					
				MgO	CaO	MnO	FeO	SrO	CO_2	total	Mg	Ca	Mn	Fe	Sr	total
BD2001-5/8	80.31	car spot (I)	siderite	1.22	2.22	3.71	54.29	0.00	38.56	100.00	0.07	0.09	0.12	1.72	0.00	2.00
BD2014-9/4A	114.60	car spot (I)	siderite	2.23	1.06	3.49	54.46	0.00	38.76	100.00	0.10	0.03	0.09	1.77	0.00	2.00
BD2014-10	126.80	car spot (I)	siderite	0.41	0.18	0.01	62.03	0.00	38.67	101.30	0.02	0.01	0.00	1.97	0.00	2.00
SGD001-8/2	241.50	core of car spot (I)	sideroplesite	13.14	0.45	1.86	42.41	0.00	41.87	99.73	0.69	0.02	0.05	1.24	0.00	2.00
BD2002-2/2A	66.45	car spot (I)	sideroplesite	17.17	0.12	0.17	39.38	0.00	43.16	100.00	0.76	0.00	0.00	1.24	0.00	2.00
BD2014-4/2A	59.50	core of car spot (I)	sideroplesite	16.27	0.03	0.25	40.59	0.00	42.87	100.01	0.72	0.00	0.01	1.28	0.00	2.00
BD2002D-3/3	209.50	car spot (I)	ankerite	11.58	29.65	1.45	12.56	0.22	44.67	100.13	0.57	1.04	0.04	0.35	0.00	2.00
BD2002B-2/2	237.80	rim of car (II)	ankerite	8.68	28.61	1.24	16.82	0.00	43.07	98.42	0.44	1.04	0.04	0.48	0.00	2.00
BD2-5/1	123.00	vein(Q)/rim (II)	ankerite	8.42	32.18	0.88	14.53	0.00	43.99	99.99	0.42	1.15	0.02	0.40	0.00	2.00
BD2002B-2/1	237.80	core of car (I)	calcite	0.12	53.42	2.17	0.46	0.00	43.73	99.90	0.01	1.92	0.06	0.01	0.00	2.00
BD2002B-3	274.70	core of car (I)	calcite	0.23	52.50	2.02	0.79	0.10	42.80	98.44	0.01	1.91	0.06	0.02	0.00	2.00
BD3001-14/5	137.00	car vein (II)	calcite	0.44	53.25	1.11	0.43	0.00	43.27	98.49	0.02	1.93	0.03	0.01	0.00	2.00

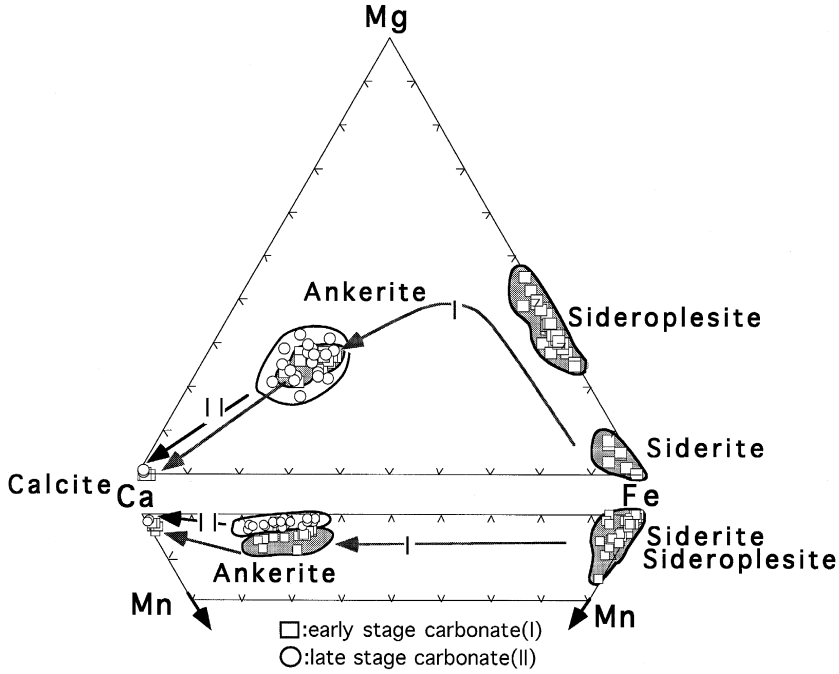

Fig. 6. Composition of carbonates and evolution trend. (I) Evolution trend of the main (early) alteration stage carbonate. (II) Evolution trend of the minor (late) alteration stage carbonate.

gites (Si/Al = 14.66–29.10) are associated with low-Mn ankerite, calcite, milky quartz and low temperature chlorites (minor/later alteration stage; Fig. 11A and C). The proportion of phengite present in the sericite probably relates to the proportion of components derived from hydrothermal solution, principally Fe^{+2} and Si. It is implied that the early stage fluids were Fe^{+2}, Si and Au-rich and the later fluids were Ca^{+2}-rich and Au-poor.

The distribution of hydrothermal chlorite along the Nell Gwynne anticline is illustrated in Fig. 11C. The temperatures derived from the chlorite compositions using chlorite geothermometry are in the range of 152 to 295°C (Cathelineau and Nieva, 1985; Kranidiotis and Maclean, 1987; Cathelineau, 1988). Temperatures from 250 to 290°C were obtained from chlorite associated with the main (early) alteration stage and lower temperatures (152–261°C) from chlorite associated with the minor (late) alteration stage nearer the core of anticline. Metamorphic temperatures of 290 to 295°C are indicated by compositions of metamorphic chlorite within the outer, western limb of the anticline. The range of temperatures is greatest in the 119500N section, probably because there is more data in this area (averages are 121750N = 282°C; 120950N = 266°C; 120500N = 275°C; 119500N = 272°C). The average temperature is highest in the 121750N section, however, there are only 4 measured samples. In the 119500N section, the lower temperatures derived from the chlorite geothermometer occur nearest the core of the anticline while the higher temperatures occur further out. This apparent temperature gradient suggests either multiple stages of fluid migration, or that fluid pathways were not perfectly restricted to the anticlinal cores.

5. Bulk rock compositional variation across the section

The concentration ranges of the elements As, Au, Pb, Cu, Zn and Hg in whole-rock samples from section 119500N are as follows: Au, ≤ 0.02–205 ppm (≤ 0.02–0.2 ppm common); As, 5 to 6100 ppm

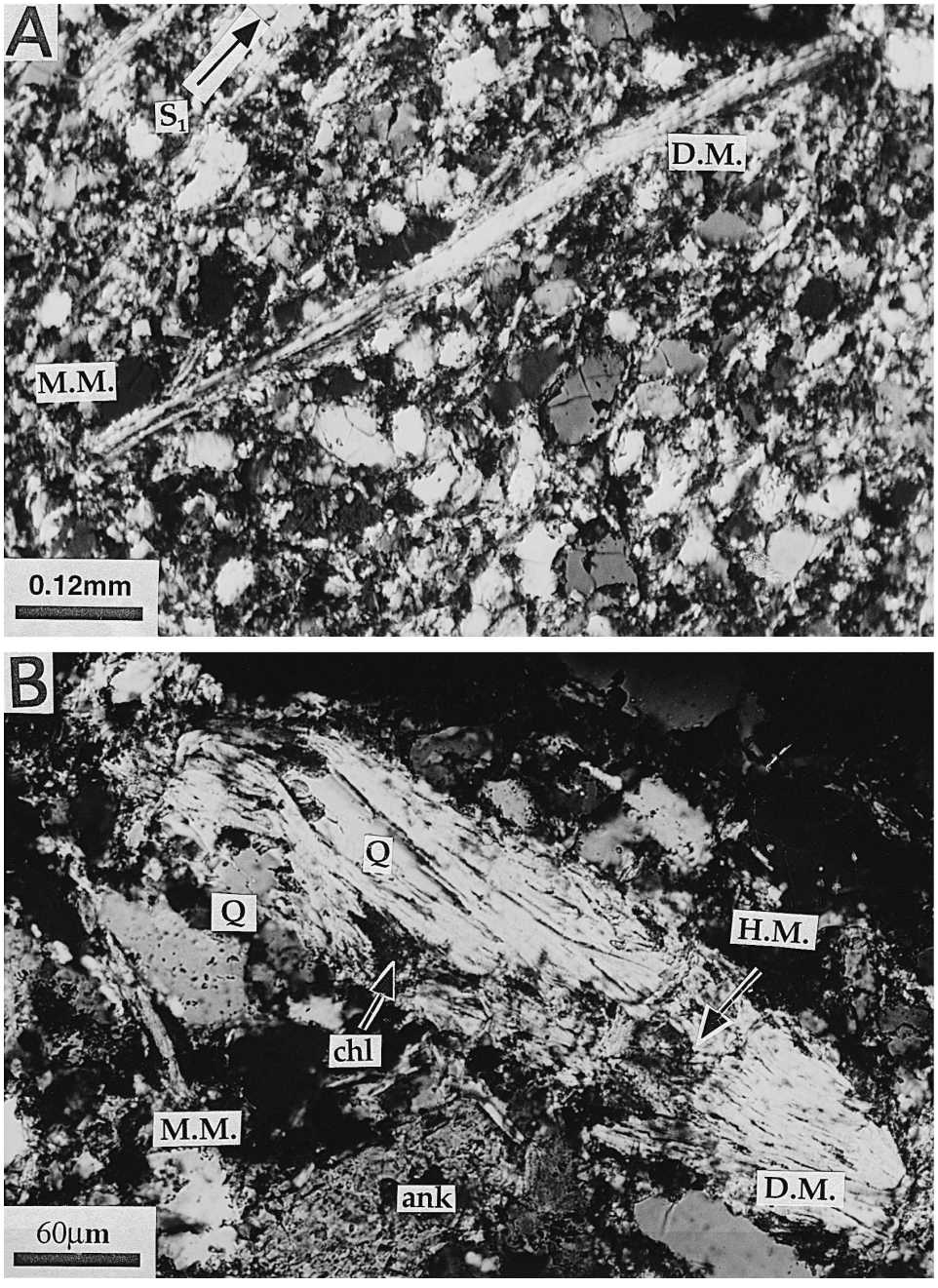

Fig. 7. Photomicrographs of mica mineral textures. (A) Detrital muscovite (D.M.), metamorphic sericite (M.M.) and hydrothermal phengitic sericite (H.M.). The orientation of the detrital muscovite probably represents the orientation of bedding, the metamorphic sericite intersects this at an acute angle while part of the detrital muscovite has been replaced by hydrothermal phengitic sericite. (B) Hydrothermal ankerite (ank), phengitic sericite (H.M.) and ripidolitic chlorite (chl) cross cutting a detrital muscovite grain. (C) Hydrothermal phengitic sericite interstitial to quartz (Q) and detrital muscovite. The hydrothermal mica shows no obvious preferred orientation. (D) Ripidolitic chlorite (chl) and carbonate (carb) replacement of detrital muscovite (D.M.). Metamorphic sericite (M.M.) is oriented at a steep angle to the elongation of the pseudomorph in the texture.

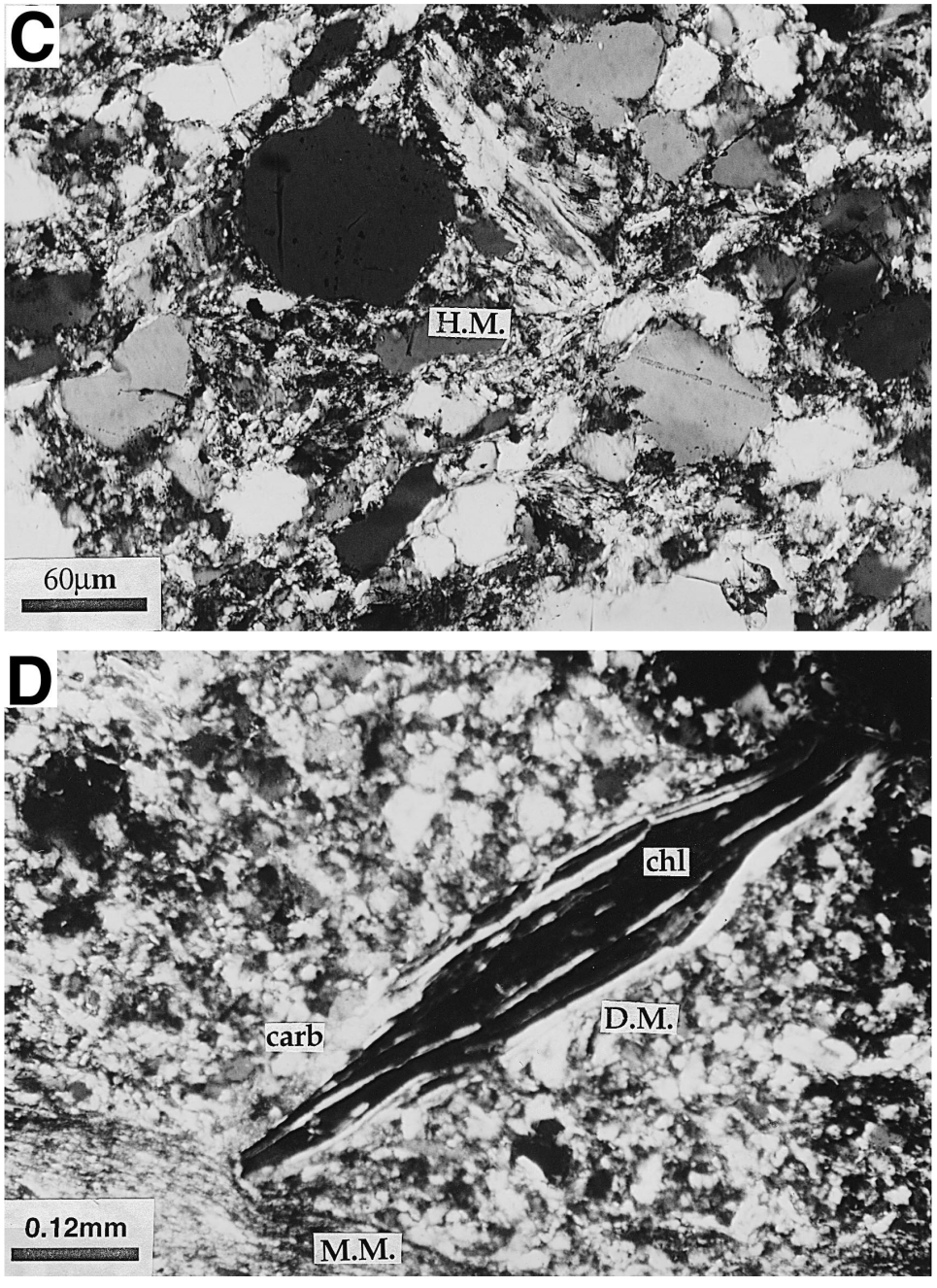

Fig. 7 (continued).

(30–100 ppm common); Cu, 5–335 ppm, (10–50 ppm common); Zn, 10–8700 ppm (50–150 ppm common); Pb, 10–2500 ppm (20–50 ppm common) and Hg, 0–130 ppm (30–60 ppm common). The spatial variation of concentrations of As, Au, Pb, Cu and Zn are illustrated by contour diagrams in Fig. 9.

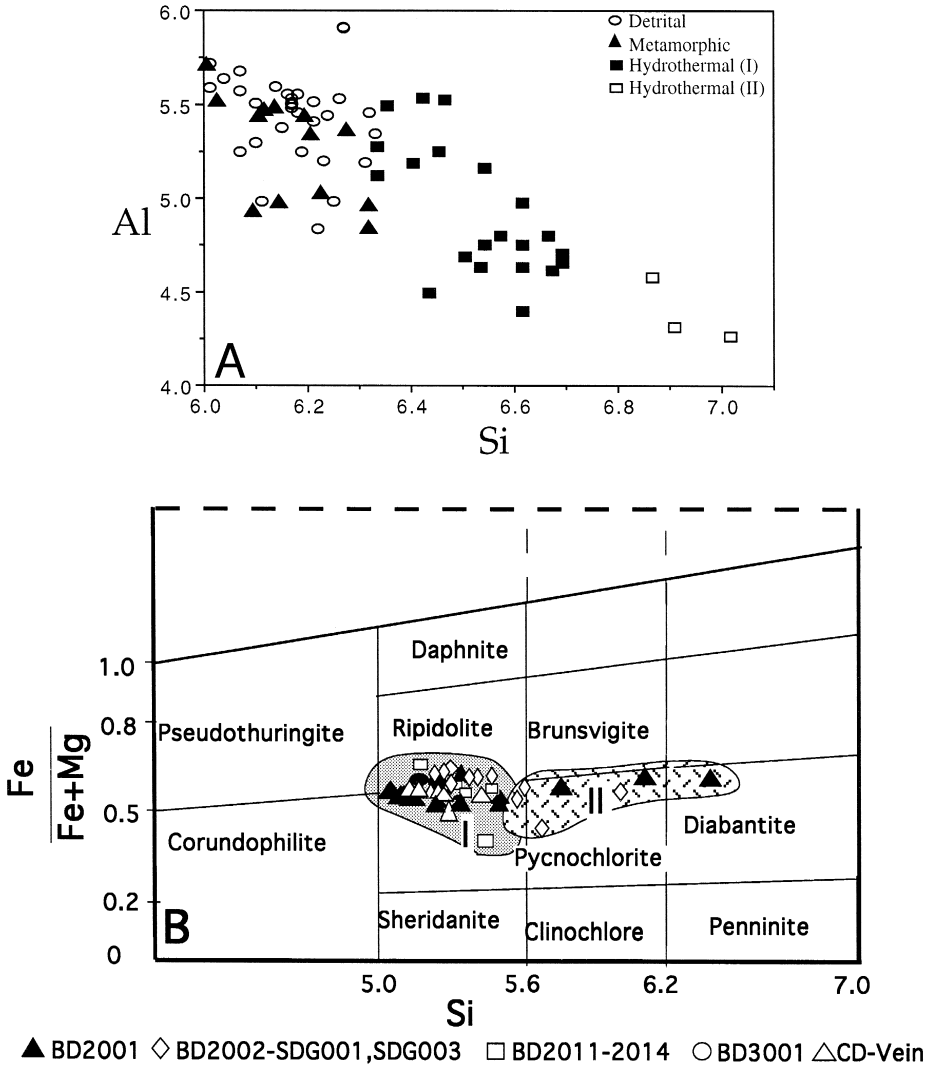

Fig. 8. Composition of muscovites/sericites and chlorites in the 119500N section. (A) Composition of detrital, metamorphic and hydrothermal mica. (B) Composition of hydrothermal chlorite. The chlorite nomenclature is after Deer et al. (1966). (I) Early stage chlorite distribution (temperature determinations after Cathelineau and Nieva, 1985, Kranidiotis and Maclean, 1987 and Cathelineau, 1988) and (II) late stage chlorite distribution.

5.1. Au

The Au grades (Fig. 9B) show a maximum in the core of the anticline associated with the classic style of mineralisation mined at Bendigo. Above this there is a zone of low gold values (in the 0.5–6.0 ppm range) in the sandstone and more silty units under massive shale units. While some of these values may be represented by auriferous veinlets, some are found in unveined sandstone (to 0.6 ppm).

5.2. As

The As concentration is highest (Fig. 9C) in the core of the anticline, corresponding to maximum Au grade, as well as in a zone above the core which is

Table 2
Representative analyses of detrital, metamorphic and two-stage hydrothermal micas (I and II)

Sample No.	BD2014-15-1	BD2014/7/1D	BD2002/4	BD2002/9/3	BD2002D/1	BD2014/7/1B	BD2001/17/1	BD2011-13-3B	BD2014-11-5B	BD2002/4/7	BD3001-14/1	BD2011/8/4
Depth (m)	208.20	96.30	155.00	211.60	134.60	96.30	246.00	215.00	164.90	155.00	137.00	158.00
Genetic type	detrital	detrital	detrital	metamorphic	metamorphic	metamorphic	hydro. (I)	hydro. (I)	hydro. (I)	hydro. (II)	hydro. (II)	hydro.(ll)
wt%												
SiO_2	46.08	48.18	45.84	44.69	46.01	45.32	48.74	47.53	48.88	51.78	53.15	52.67
TiO_2	0.43	0.52	0.32	1.01	0.79	0.99	0.24	0.22	0.39	0.25	0.18	0.27
Al_2O_3	35.67	35.27	34.67	33.97	33.53	34.52	28.96	29.08	30.19	30.38	27.32	27.87
FeO	0.95	1.15	1.85	3.02	1.22	3.36	2.44	3.43	2.31	1.81	3.18	3.20
MnO	0.00	0.04	0.05	0.01	0.03	0.01	0.03	0.02	0.05	0.02	0.00	0.03
MgO	0.68	1.13	0.77	0.82	0.93	0.64	3.25	2.52	2.31	1.89	2.33	2.89
CaO	0.00	0.00	0.00	0.06	0.00	0.00	0.00	0.00	0.00	0.00	0.03	0.00
Na_2O	1.29	0.31	0.49	0.39	0.60	0.50	0.00	0.27	0.18	0.19	0.14	0.26
K_2O	9.38	7.86	10.68	9.62	9.31	8.54	10.25	10.77	10.82	9.88	8.22	7.31
ZnO	0.00	0.00	0.00	0.00	0.00	0.08	0.03	0.00	0.00	0.02	0.20	0.05
Cr_2O_3	0.01	0.06	0.01	0.00	0.00	0.04	0.06	0.00	0.00	0.00	0.04	0.01
P_2O_5	0.01	0.00	0.00	0.00	0.00	0.01	0.00	0.01	0.00	—	—	0.00
S	0.00	0.01	0.00	0.00	0.00	0.01	0.00	0.00	0.02	—	—	0.03
F	0.13	0.05	0.00	0.00	0.00	0.08	0.00	0.21	0.09	—	—	0.37
Cl	0.01	0.00	0.00	0.00	0.00	0.02	0.00	0.00	0.02	—	—	0.01
Total	94.66	94.60	94.70	93.59	92.41	94.11	93.99	94.07	95.27	96.21	94.79	94.95
nos cation							based on 22 (O)					
Si	6.14	6.32	6.17	6.10	6.27	6.11	6.60	6.50	6.54	6.76	7.02	6.91
Al(IV)	1.86	1.68	1.83	1.90	1.73	1.89	1.40	1.50	1.46	1.24	0.98	1.09
Al(VI)	3.74	3.78	3.67	3.56	3.66	3.60	3.22	3.19	3.30	3.44	3.28	3.23
Ti	0.04	0.05	0.03	0.10	0.08	0.10	0.02	0.02	0.04	0.02	0.02	0.03
Fe	0.11	0.13	0.21	0.34	0.14	0.38	0.28	0.39	0.26	0.20	0.35	0.35
Mn	0.00	0.00	0.01	0.00	0.00	0.00	0.00	0.00	0.01	0.00	0.00	0.00
Mg	0.14	0.22	0.15	0.17	0.19	0.13	0.66	0.51	0.46	0.37	0.46	0.57
Cr	0.00	0.01	0.00	0.00	0.00	0.00	0.01	0.00	0.00	0.00	0.00	0.00
Ca	0.00	0.00	0.00	0.01	0.00	0.00	0.00	0.00	0.00	0.00	0.00	0.00
Na	0.33	0.08	0.13	0.10	0.17	0.13	0.00	0.07	0.05	0.05	0.04	0.07
K	1.59	1.32	1.83	1.67	1.76	1.47	1.77	1.88	1.85	1.65	1.39	1.22
Total	13.95	13.58	14.03	13.95	13.85	13.82	13.95	14.07	13.96	13.72	13.53	13.46
Si/Al(IV)	3.30	3.77	3.37	3.20	3.62	3.24	4.70	4.33	4.48	5.46	7.20	6.36
Fe+Mg/ Al(VI)	0.06	0.09	0.10	0.14	0.09	0.14	0.29	0.28	0.22	0.16	0.25	0.28

Table 3
Representative analyses of two stage hydrothermal chlorites (I and II)

Sample No.:	BD2001-5/4	BD2001-15	BD2001-17	BD2011-9	BD2011-9	BD2011-13-2A	BD2014-15-4	BD3001-21/4	BD3001-14/2	BD2002/9/5	BD2001/5/5	BD2001/17
depth (m):	80.31	209.7	246	168.7	168.7	215	208.2	200	137	211.60	80.31	246.00
description:	Chl-car(I)	Chl-car(I)	chl-ser(I)	Chl-car(I)	Chl-Q(I)	Chl-Q(I)	Chl-O(I)	Chl-Q(I)	Chl cut by S2(I)	Chl(II)	Chl(II)	Chl(II)
(wt%)												
SiO_2	26.69	24.12	23.61	24.00	25.38	24.18	23.29	23.75	24.02	29.10	29.49	32.16
TiO_2	0.11	0.06	0.05	0.04	0.07	0.02	0.08	0.08	0.04	0.45	0.06	0.12
Al_2O_3	22.41	21.90	21.66	21.51	22.78	21.39	21.71	21.36	22.30	22.93	25.22	26.43
FeO	25.05	27.82	28.69	27.38	26.46	27.00	31.96	28.75	31.40	23.24	21.41	19.78
MnO	0.14	0.26	0.24	0.09	0.17	0.13	0.29	0.23	0.30	0.16	0.13	0.18
MgO	9.60	12.25	12.60	10.92	10.95	12.18	9.04	12.70	11.10	10.38	8.26	7.82
CaO	0.01	0.00	0.05	0.03	0.02	0.03	0.04	0.00	0.01	0.02	0.00	0.00
Na_2O	0.13	0.06	0.00	0.05	0.11	0.02	0.01	0.02	0.01	0.12	0.00	0.00
K_2O	1.16	0.00	0.04	0.04	0.12	0.06	0.02	0.01	0.01	0.99	1.24	0.03
P_2O_5	0.00	0.00	0.00	0.03	0.07	0.00	0.01	0.00	0.00	0.00	0.02	0.00
Cr_2O_3	0.04	0.01	0.00	0.00	0.03	0.00	0.00	0.00	0.00	0.00	0.00	0.00
S	0.00	0.00	—	0.00	0.01	0.00	0.00	—	—	—	0.03	—
F	0.52	0.08	—	0.05	0.00	0.09	0.02	—	—	—	0.04	—
Cl	0.04	0.01	—	0.02	0.04	0.02	0.01	—	—	—	0.02	—
ZnO	0.01	0.09	0.02	0.01	0.09	0.00	0.20	0.05	0.00	0.00	0.00	0.07
Total	85.8991	86.569	86.95	84.16	86.30	85.11	86.67	86.95	89.19	87.41	85.91	86.58
No.'s cation where (OH) is given as 16.0, formula has been calculated on the basis on 28 oxygen equivalents ignoring H_2O												
Si	5.73	5.24	5.12	5.35	5.46	5.32	5.19	5.15	5.14	6.01	6.12	6.45
Ti	0.02	0.01	0.01	0.01	0.01	0.00	0.01	0.01	0.01	0.07	0.01	0.02
Al(IV)	2.27	2.76	2.88	2.65	2.54	2.68	2.81	2.85	2.86	1.99	1.88	1.55
Al(VI)	3.41	2.84	2.65	3.00	3.24	2.86	2.89	2.61	2.77	3.59	4.29	4.70
Fe^{3+}	0.00	0.00	0.22	0.00	0.00	0.00	0.00	0.22	0.08	0.00	0.00	0.00
Fe^{2+}	4.50	5.05	4.98	5.10	4.76	4.97	5.96	5.00	5.54	4.01	3.71	3.32
Mn	0.02	0.05	0.04	0.02	0.03	0.02	0.05	0.04	0.05	0.11	0.02	0.03
Mg	3.07	3.96	4.07	3.63	3.51	3.99	3.00	4.11	3.54	3.19	2.55	2.34
Ca	0.00	0.00	0.01	0.01	0.01	0.01	0.01	0.00	0.00	0.00	0.00	0.00
Na	0.06	0.02	0.00	0.02	0.05	0.01	0.00	0.01	0.00	0.05	0.33	0.00
K	0.32	0.00	0.01	0.01	0.03	0.02	0.01	0.00	0.00	0.26	0.00	0.01
P	0.00	0.00	—	0.00	0.01	0.00	0.00	—	—	—	0.00	—
Cr	0.01	0.00	—	0.00	0.01	0.00	0.00	—	—	—	0.00	—
Total	19.41	19.94	20.00	19.81	19.65	19.89	19.94	20.00	20.00	19.29	18.92	18.41
T-Bendigo	226.46	281.12	293.48	269.18	256.61	272.79	280.50	290.05	288.32	199.52	185.75	151.45

generally discordant to the hydrothermal alteration zoning patterns. Although some of the latter As zone may be due to dispersal during weathering and oxidation, this is not the case below 50 m. This indicates that there were at least two periods of arsenic and gold introduction, an early phase where As is restricted to the veins and areas immediately around the veins in the saddle reef position and at least one later phase where As and minor Au mineralisation cross-cuts the earlier phase of mineralisation.

5.3. Cu

The distribution of Cu in the section (Fig. 9D) is highly erratic although the highest values (~ 60 ppm) correspond closely to the Au maximum in the core of the anticline.

5.4. Zn

The distribution of Zn (Fig. 9E) is again erratic, although higher values (~ 200 ppm) generally correspond to the anomalous Au. However, the highest values were found in a sample in the synclinal area, unrelated to anomalous gold.

5.5. Pb

The distribution of Pb is, in part, closely correlated to As (Fig. 9C and F), as it enters readily into arsenopyrite. There is a maximum slightly to the east of the Au and As maximum (> 200 ppm) in the core of the anticline and a series of maxima above the core area. The latter correspond to As maxima and were possibly from an unidentified fault and/or vein zone.

5.6. CO_2

This parameter was determined to confirm the distribution of carbonate. As can be seen (Fig. 9G), CO_2 values closely correspond to the distribution of carbonate minerals determined by petrographic methods. This is a useful exploration parameter as the analysis of CO_2 is easy and relatively inexpensive.

5.7. H_2O^+

This parameter was determined to see if the extent of hydrous mineral alteration could be determined analytically. This was clearly not useful (Fig. 9H), probably because H_2O^+ values in the weathered and oxidised zone (generally within 50 m of the surface) are very erratic as well as the proportion of hydrous minerals of detrital and metamorphic origin being nonsystematic.

6. Discussions and conclusions

This study has established the following general observations:

(1) Most of the Nell Gwynne mineralisation occurs in a saddle reef position within an anticlinal structure and mainly just beneath a thick shale unit. There is disseminated and vein mineralisation present in the sandstones above the main shale unit, particularly below shale units higher in the sequence (Fig. 12).

(2) Much of the quartz in the saddle reef has been sheared to varying degrees. The orientation of the shearing is generally at a steep angle, parallel or sub-parallel to the axial plane.

(3) The carbonates include siderite, sideroplesite and ankerite, calcite; sericite is phengite and chlorite is ripidolite and pycnochlorite.

(4) There is a systematic zoning of the volumetric proportions of the carbonate, phengitic sericite, chlorite and sulphide alteration minerals around the saddle reef structure in the 119500N section and along the axis of the anticline.

(5) Going out from the saddle reef, first carbonate (at 50 to 130 m); then chlorite (at 100 m), hydrothermal sulphides (at 90 to 140 m); and finally phengitic sericite (at > 150 m) are lost from the alteration mineral assemblages.

(6) Generally, the carbonate compositions progress from being Fe-rich early in the paragenesis to Fe-poor during the later stage in the two different alteration periods, I: siderite $\rightarrow$ sideroplesite $\rightarrow$ ankerite$_{I}$ $\rightarrow$ calcite$_{I}$ and II: ankerite$_{II}$ $\rightarrow$ calcite$_{II}$ (Fig. 6).

(7) The apex of the dome has the highest proportion of Fe-rich carbonate but no significant variations

exist with respect to chlorite and sericite–phengite compositions.

(8) Chalcopyrite, sphalerite and pyrite occur in veins as euhedral crystals (in the case of pyrite) and in spheroidal masses (framboids) 90 to 140 m above the saddle reef.

(9) Arsenopyrite with Au occurs in the saddle reef position (core of the anticline) but arsenopyrite and Au also occur in a zone above the saddle reef position. This second area of high As cross-cuts the general alteration zoning. The Pb anomaly coincidental with this second As anomaly reflects the fact that Pb is often found as a solid solution in arsenopyrite.

(10) Cu shows only a poor correlation with Au in the area of the saddle reef while Zn and H_2O^+ shows no obvious relationships to Au. CO_2 correlates well with the extent of carbonate distribution determined by petrographic methods.

The saddle reef mineralisation occurs at an interface between a sandstone and a thick shale unit. The view taken is that the shale functioned as an impermeable 'choke' on the mineralisation (also see Kwak

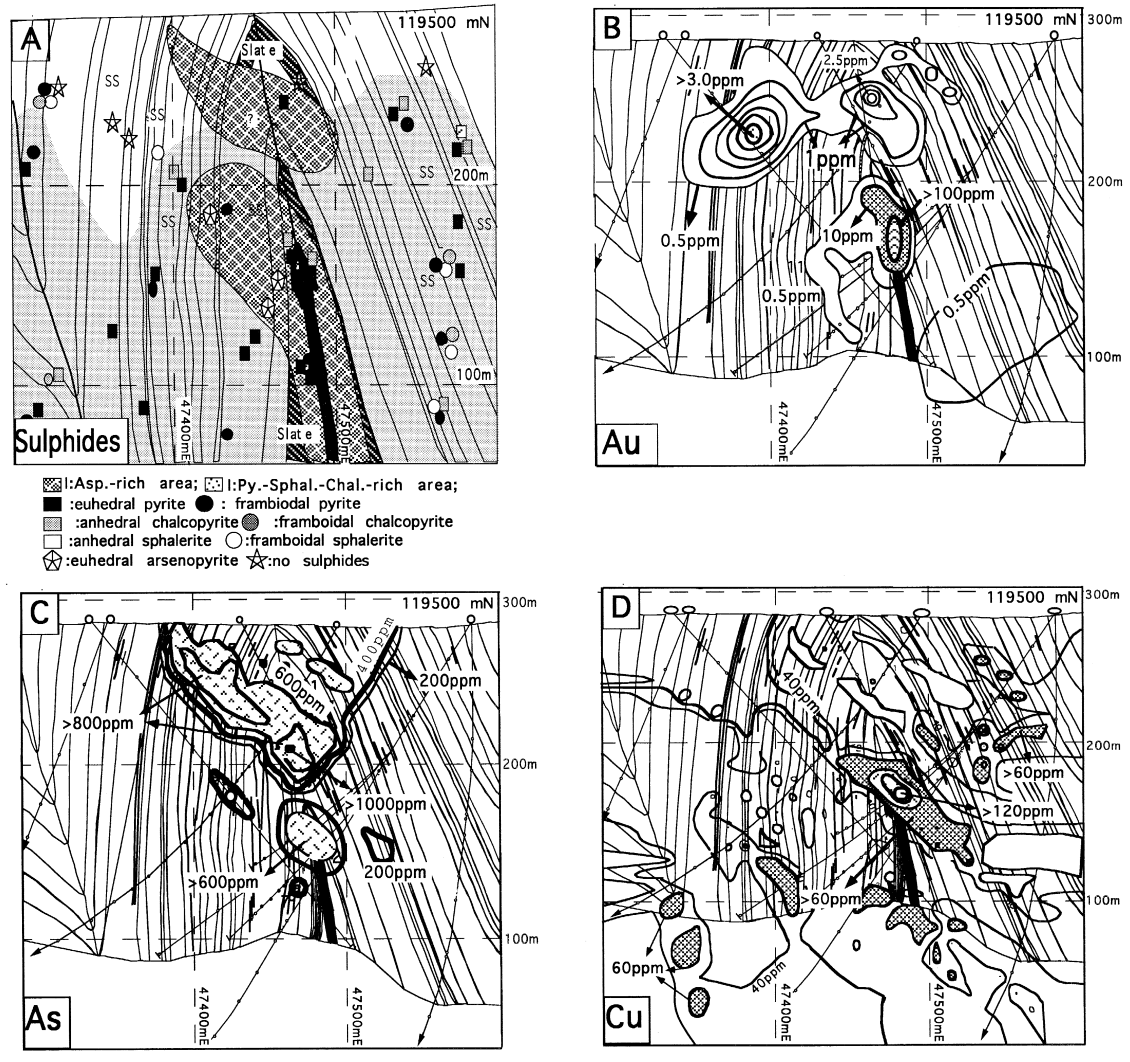

Fig. 9. Distribution of sulphides (A), Au (B), As (C), Cu (D), Zn (E), Pb (F), CO_2 (G) and H_2O^+ (H) in the 119500N section. See text for description.

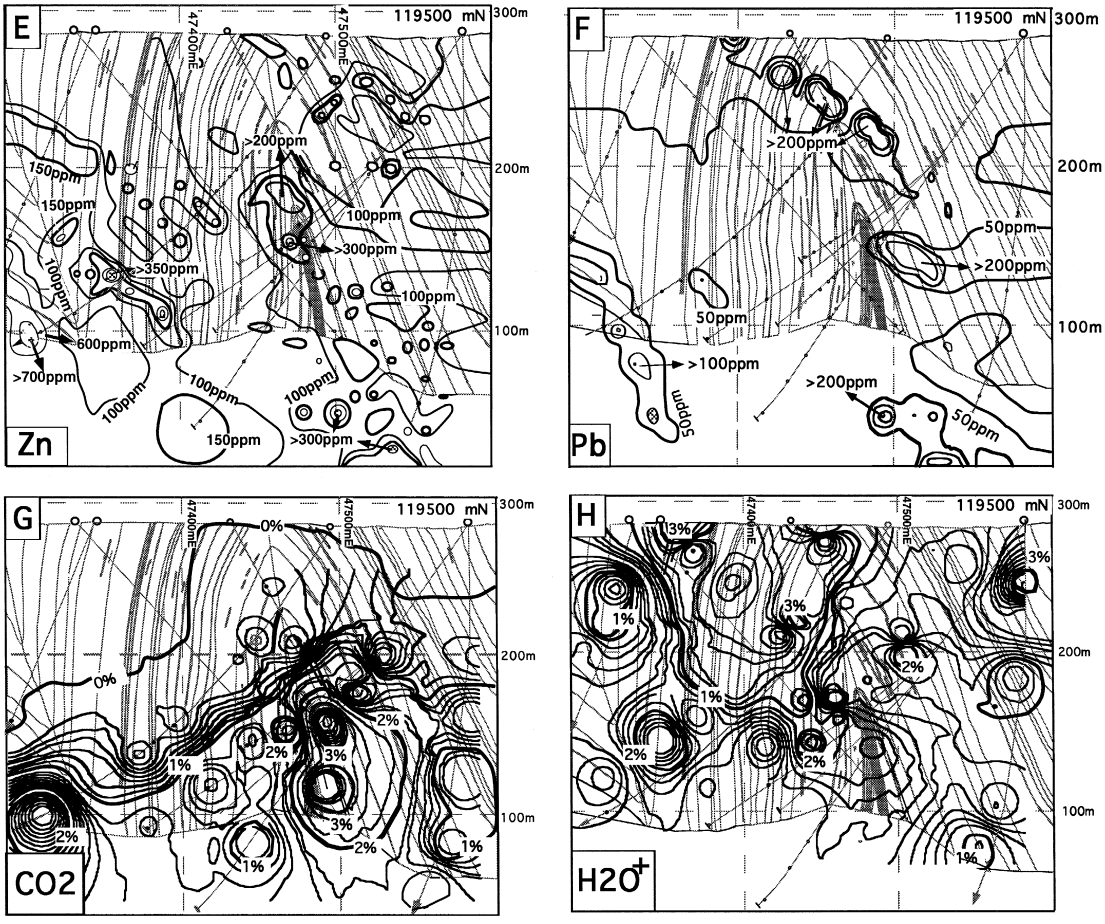

Fig. 9 (continued).

and Roberts, 1996). The shale–sandstone interface was an area of low pressure during mineralisation with the choke restricting the flow of ore fluids. The function of an impermeable 'choke' and the reduction of the ore fluids by the graphite present in the shale lead to the precipitation of gold (and carbonate). Enough fluid passed this barrier, probably during a later period of ore genesis, to produce the As–Pb–Au mineralisation found in the overlying sandstones.

Wall rock alteration has generally been thought to be relatively restricted in area around central Victorian gold deposits, although alteration at Bendigo has previously been viewed as being more widespread (Cox et al., 1991). The following widths of alteration have been observed at the following deposits (after Gao and Kwak, 1997): Maxwells, probably at less than 20 m; New Cambrian, 8 m; Wattle Gully, 10 m and Costerfield, 5 m. Some of these may be wider as the widths were determined mainly by bulk chemical analyses of available samples. At Bendigo the alteration halo is at least 150 m wide (extent of sericite zone). From the information presented here and by Gao and Kwak (1996, 1997) it appears that, to a first approximation, the width of the alteration zone is proportional to the size of the deposit. The Maxwells, New Cambrian and Wattle Gully deposits produced between 1 and 12 tonne of gold each and have alteration zones of 8 to 20 m. The Brunswick deposit has produced only 21 kg of gold although current mining would greatly increase this value. The alteration zone at Brunswick is only 5 m wide. Thus, of

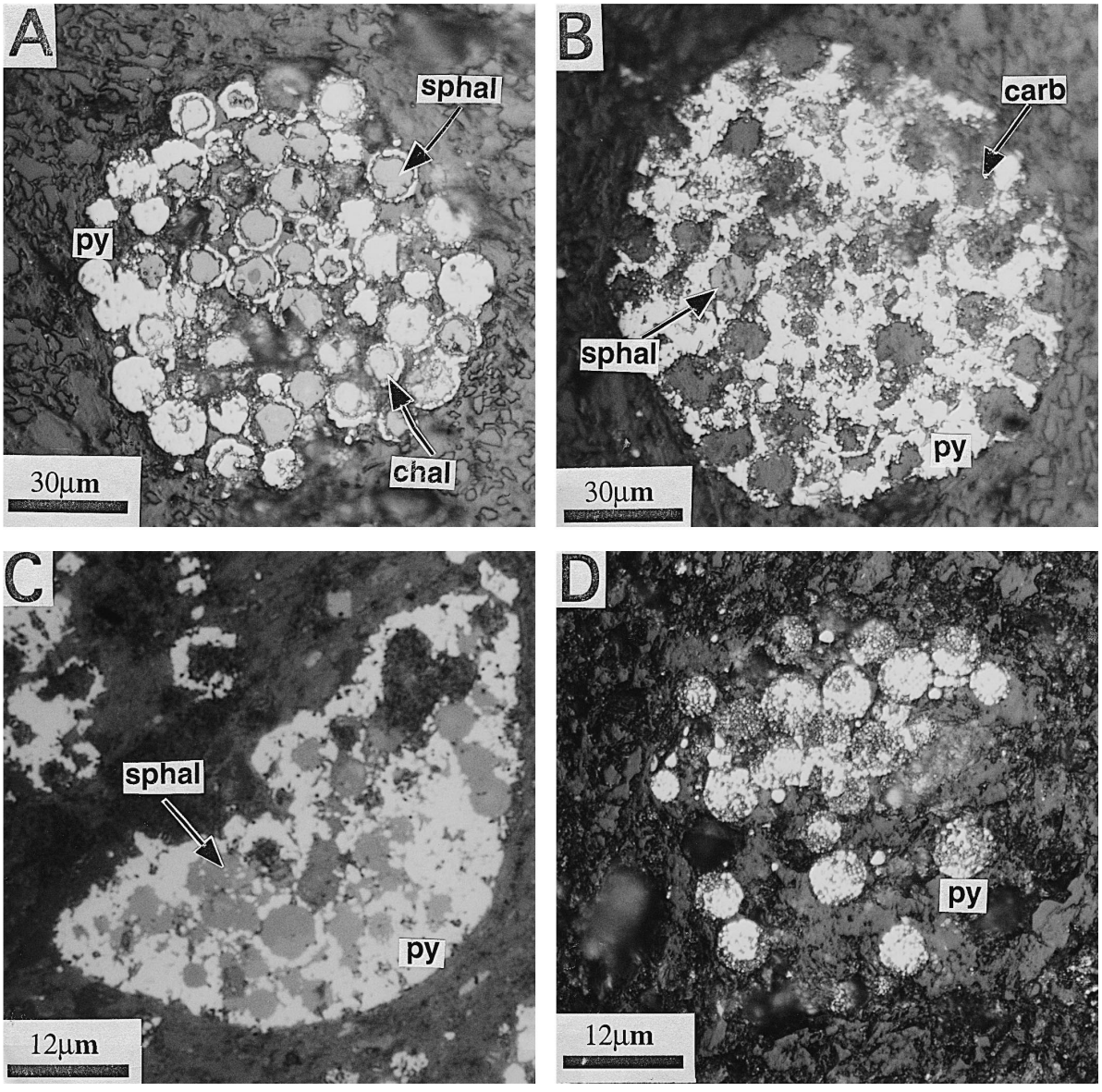

Fig. 10. Photomicrographs of framboidal/spheroidal sulphides. (A) A spheroidal body consisting of chalcopyrite (chal) and sphalerite (sphal) spheroids each mantled by pyrite (py). There are also a number unidentified grains present. (B) A spheroidal body consisting of sphalerite (sphal) and carbonate (carb) spheroids and large crystal of pyrite (py). (C) Part of a spheroidal body consisting of sphalerite spheroids included in pyrite (py). (D) Framboidal pyrite (py) showing an unusual, internal cell-like structure with each spheroid composed of a mass of smaller spheroids.

all the Victorian deposits on which detailed work is available, the Bendigo deposits have both the widest alteration halo and the highest gold content. The Bendigo gold field has produced 684 tonne of gold while the Nell Gwynne anticline in the field has produced 6.17 tonne. Thus, the width of the alteration zone is believed to be proportional to the size of the gold deposit.

There appears to be two periods of mineralisation, one producing the saddle reef-style and the other

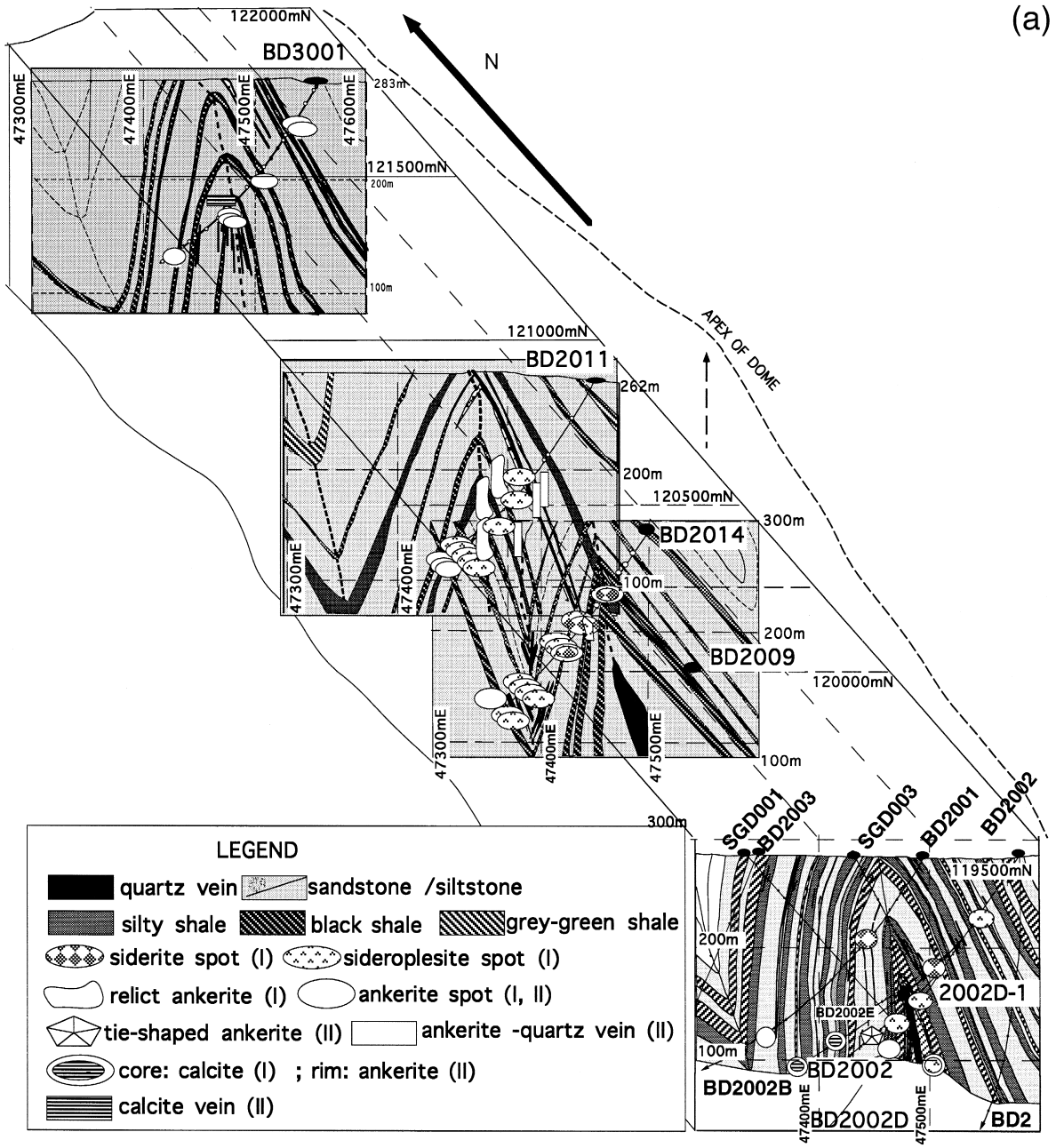

Fig. 11. The distribution of carbonate, sericite and chlorite, mainly in the axial plane of the Nell Gwynne anticlinal dome. (A) The distribution of different compositional and textural types of carbonate in the Nell Gwynne anticlinal dome. (B) The variation of the phengitic component in hydrothermal mica. The Si:Al (IV) ratio greater than 3:1 is a measure of the proportion of phengite present. (C) The distribution of chlorite with the estimated formation temperatures using the method of Cathelineau and Nieva (1985), Kranidiotis and Maclean (1987) and Cathelineau (1988).

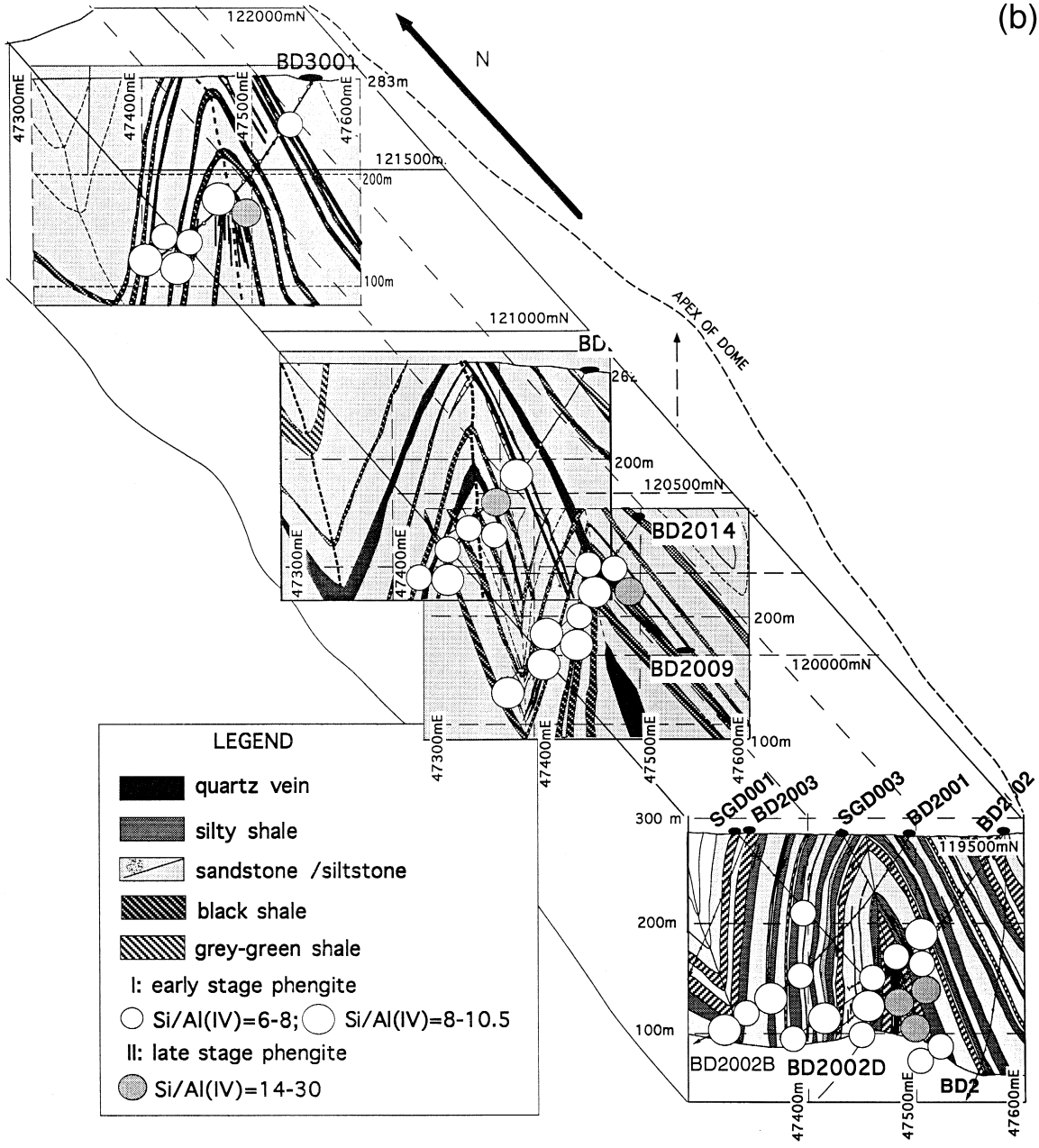

Fig. 11 (continued).

producing high As and much lower Au values hosted more commonly in the sandstone units. The latter cross-cuts the former (Fig. 12) although both occupy the axial zones of the anticlinal structures. Preliminary data using common lead for dating galena in contact with gold in the veins yielded a model age of approximately 430 Ma while arsenopyrite yielded an age of approximately 350 Ma (Kwak and Maas,

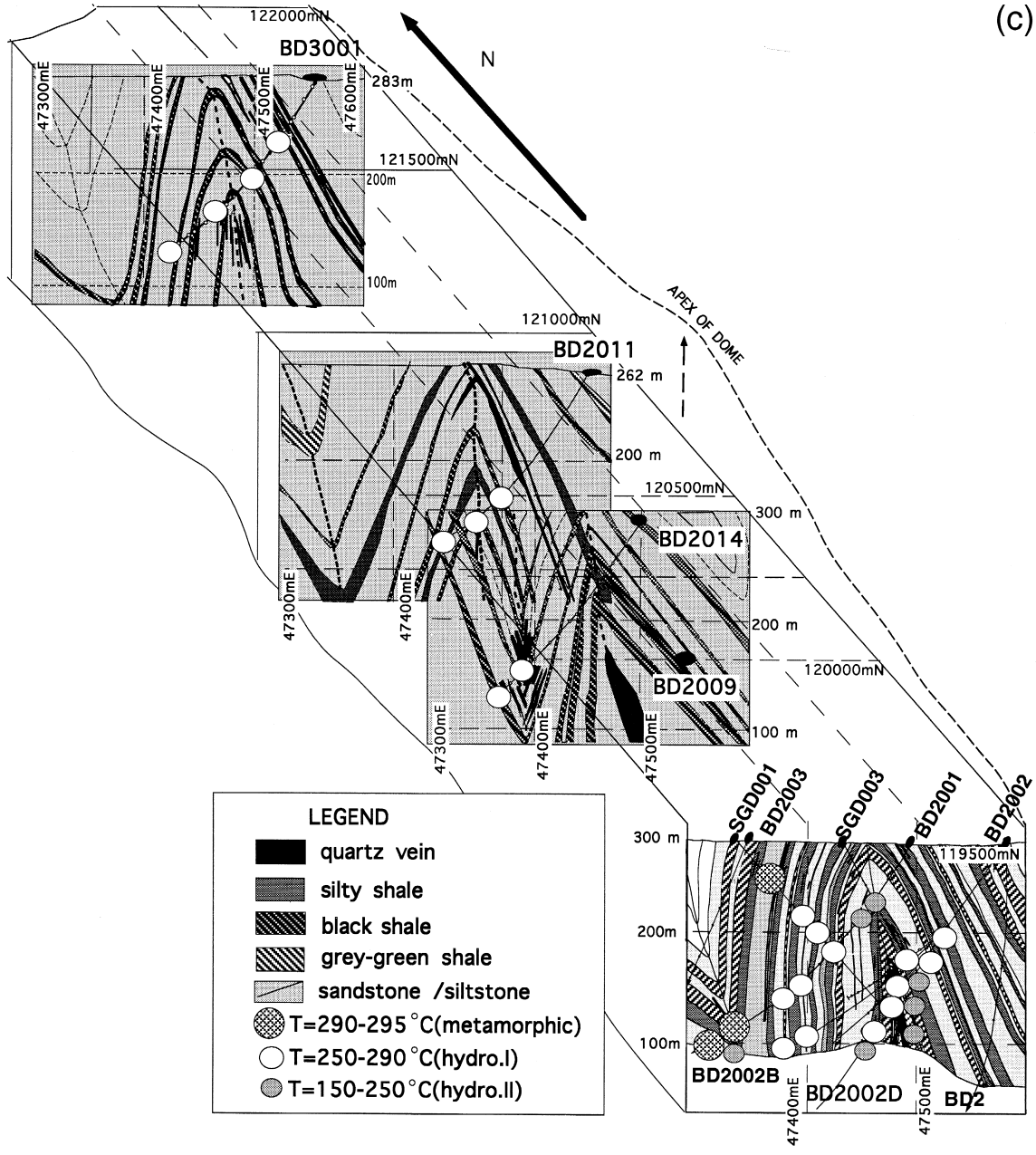

Fig. 11 (continued).

1996, study in progress). The axial areas of the anticlinal domes probably have been the loci for deposition (hydrothermal and magmatic) at least two and probably three times. This is consistent with the views of other workers (e.g. McCuiag and Kerrich, 1994) who state that ‘‘many deposits have evolved through a number of pressure–temperature regimes and fluid events’’.

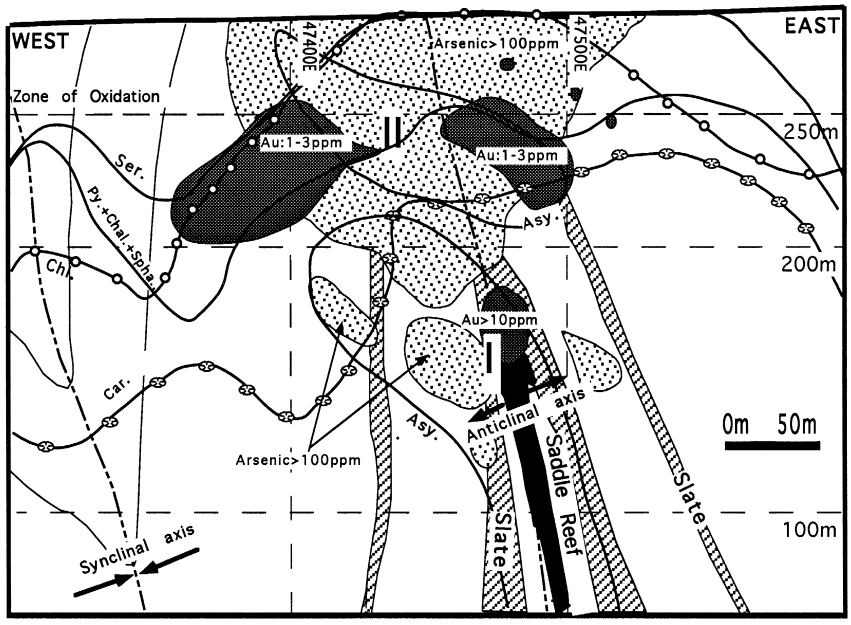

Fig. 12. A compilation of data in Figs. 4 and 9 showing the saddle reef-style mineralisation and the cross-cutting nature of the late As (-Pb–Au) plume-like mineralisation. The latter is interpreted to represent a later period of mineralisation.

The fact that the sulphide spheroids or framboids, shown in Fig. 10A to C, tend to occur both with hydrothermal alteration minerals and in a broad halo around the saddle reef may indicate that they were produced by replacement of framboids similar to those shown in Fig. 10D, or that they represent accumulations of sedimentary origin. The framboidal sulphide (Fig. 10D) may or may not have been pyrite prior to mineralisation. It may have been marcasite or, as in modern sediments, sedimentary framboidal Fe-sulphides may first have formed as greigite (Fe_3S_4) and later recrystallised as the more stable pyrite or pyrrhotite (Sweeney and Kaplan, 1973; Fenchel and Blackburn, 1979). The framboids in this study were too fine-grained to analyse by X-ray means and this could not be confirmed.

Another possibility is that the unusual sulphide framboids (or spheroids) are of primary sedimentary origin. If this were to be the case, then a model is possible whereby the Bendigo deposits were formed by the redistribution of gold and other metals derived from the spheroids in the sandstones and from locally derived shales. Hydrothermal alteration by fluids derived from other sources may still have affected the host rocks immediately around the saddle reefs, mixing hydrothermal products such as carbonate, sericite and chlorite with the spheroids and their altered equivalents. Prior to the 1920's various authors (e.g. Dunn, 1896) held the view that a favourable bed, or beds, near the upper Bendigonian of the Ordovician sequence contained the best gold values. This is, or is close to, the unit containing the spheroids (Bendigonian–Chewtonian boundary): A feature which supports the 'favourable bed' theory.

7. Application to exploration

A summary of the features found in this study which could be used as a guide to exploration for deposits similar to those at Bendigo is given below. Of these, the following are probably the most useful for locating a large Bendigo-style deposit:

(a) An extensive zone of hydrothermal alteration is needed; probably the larger and more intense the alteration, the larger the deposit.

(b) Sericite and chlorite alteration extend well beyond carbonate alteration, the style generally thought of as the most useful exploration guide. As

sericite has K present, radiometric surveys may indicate areas of such alteration.

(c) The As and Au distributions show that very high As anomalies do not necessarily coincide with areas of high anomalous gold. As indicates anomalous Au is present but the geochemistry of Au during deposition is clearly different from that of As.

(d) A thick shale unit, or other geological feature to facilitate a choke mechanism may be required. This can also be produced by the precipitation of vein minerals.

(e) Doubly plunging, near-isoclinal anticlinal or steep chevron structures (domes) are required.

(f) A mechanism of 'locking' is envisioned where compressive stress can no longer be taken up by folding beyond the point where it is isoclinal and subsequent shortening can not continue without changing stress directions. Continued compression then produces reverse faulting at acute angles to the maximum (-minimum) principal stress (plane), particularly near the apices of the anticlinal domes. These have been the areas of maximum widths of mineable gold mineralisation at Bendigo.

(g) The occurrence of framboid-like bodies containing Cu, Zn, Ni, Sb and Au may be a requirement.

Acknowledgements

We are greatly indebted to Bendigo Mining N.L. for their help in providing samples, visits underground in the Deborah dome, and financial support. Xia Li's work was supported by the Aus AID Commonwealth scholarship plan.

References

Ames, D.E., Franklin, J.M., Potts, P.J., 1991. Zonation of hydrothermal alteration at the San Antonio gold mine, Bissett, Manitoba, Canada. Econ. Geol. 86, 600–619.

Bouma, A.H., 1962. Sedimentology of some Flysch Deposits. A Graphic Approach to Facies Interpretation. Elsevier, Amsterdam.

Bowen, K.G., 1972. Arsenic as a guide to gold mineralisation at the Wattle Gully and Sambas mines. Min. Geol. J. Vic. 7 (2), 5–15.

Cas, R.A.F., 1983. A review of the paleogeographic and tectonic development of the Palaeozoic Lachlan Fold Belt of southeastern Australia. Geol. Soc. Aust. Spec. Publ. 10, 1–104.

Cas, R.A.F., VandenBerg, A.H.M., 1988. Ordovician. In: Douglas, J.G., Ferguson, J.A. (Eds.), Geology of Victoria. Geol. Soc. Aust. Spec. Publ., pp. 63–102.

Cathelineau, M., 1988. Cation site occupancy in chlorites and illites as a function of temperature. Clay Miner. 23, 475–485.

Cathelineau, M., Nieva, D., 1985. A chlorite solid solution geothermometer. The Los Azufres (Mexico) geothermal system. Contrib. Mineral. Petrol. 91, 235–244.

Cox, S.F., Wall, V.J., Etheridge, M.A., Potter, T.F., 1991. Deformational and metamorphic processes in the formation of mesothermal vein-hosted gold deposits-examples from the Lachlan Fold Belt in central Victoria, Australia. Ore Geol. Rev. 6, 391–423.

Cox, S.F., Sun, S.S., Etheridge, M.A., Wall, V.J., Potter, T.F., 1995. Structural and geochemical controls on the development of turbidite-hosted gold quartz vein deposits, Wattle Gully Mine, central Victoria, Australia. Econ. Geol. 90, 1722–1746.

Dunn, E.J., 1896. Reports on the Bendigo Goldfield. Spec. Rep. Mines Dep. Vic.

Fenchel, T., Blackburn, T.H., 1979. Bacteria and Mineral Cycling. Academic Press, London NW, pp. 131–142.

Gao, Z.L., Kwak, T.A.P., 1996. Turbidite-hosted gold deposits in the Bendigo–Ballarat and Melbourne zones, Australia. I. Geology, mineralisation, stable isotopes and implications for exploration. Int. Geol. Rev. 37, 910–944.

Gao, Z.L., Kwak, T.A.P., 1997. The geochemistry of wall rock alteration in turbidite-hosted gold vein deposits, central Victoria. Australia. J. Geochem. Explor. 59, 259–274.

Groves, D.I., Barley, ME, Barnicoat, A.C., Cassidy, K.F., Fare, R.J., Hagerman, S.G., Ho, S.E., Hornsky, J.M.A., Mikucki, E.J., Mueller, A.G., McNaughton, N.J., Perring, C.S., Ridley, J.R., Vearncombe, J.R., 1992. Sub-greenschist to granulite-hosted Archaean gold deposits of the Yilgarn Craton: A depositional continuum from deep-sourced hydrothermal fluids in crustal-scale plumbing systems. In: Groves, J.E., Ho, S.E. (Eds.), The Archaean; Terrains, Processes, and Metallogeny. Geol. Dept. (Key Centre) Univ. Ext., Univ. West. Aust. Publ. 22, 325–337.

Deer, W.A., Howie, R.A., Zussman, J., 1966. An Introduction to the Rock Forming Minerals. Longman Group, London, pp. 231–241.

Kontak, D.J., Smith, P.K., Kerrich, R., Williams, P.F., 1990. Integrated model for Meguma group gold deposits, Nova Scotia, Canada. Geology 18, 238–242.

Kranidiotis, P., Maclean, W.H., 1987. Systematics of chlorite alteration at the Phelps Dodge massive sulphide deposit, Matagami, Quebec. Econ. Geol. 82, 1898–1911.

Kuhns, R.J., 1986. Alteration styles and trace element dispersion associated with the Golden Giant deposit, Ontario, Canada. In: MacDonald, A.J. (Ed.), Proceedings of Gold '88. An International Symposium on the Geology of Gold. Toronto, pp. 340–354.

Kwak, T.A.P., Roberts, C., 1996. Sandstone-hosted gold deposits, Victoria, Australia. A new exploration target: Recent developments in Victorian geology and mineralisation. Aust. Inst. Geol. Bull. 20, 63–69.

Love, D.A., Roberts, R.G., 1991. The geology and geochemistry

of gold mineralisation and associated alteration at the Rundle gold deposit, Abitibi Subprovince, Ontario. Econ. Geol. 86, 644–666.

McCuiag T.C., Kerrich, R., 1994. $P-T-t$ Deformation characteristics of lode gold deposits: Evidence from alteration systems. In: Lentz, D.R. (Ed.), Alteration and Alteration Processes associated with Ore-forming Systems, vol. 11. Short Course Notes, Geol. Assoc. Can., pp. 339–380.

Mueller, A.G., Groves, D.I., 1991. The classification of western Australian greenstone-hosted gold deposits according to wall-rock alteration mineral assemblages. Ore Geol. Rev. 6, 291–331.

Phillips, G.N., Powell, R., 1992. Gold only Provinces and their Common Features. Contribution 43. Nat. Key Centre in Econ. Geol. and Geol. Dept., James Cook Univ. of N. Qld., 18 pp.

Sharpe, E.N., MacGeehan, P.J., 1990. Bendigo goldfield. In: Hughes, F.E. (Ed.), Geology of the Mineral Deposits of Australia and Papua New Guinea. Australas. Inst. Min. Metall., pp. 1287–1296.

Sketchley, D.A., Sinclair, A.J., 1991. Carbonate alteration in Basalt, Total Erickson Gold Mine, Cassiar, northern British Columbia, Canada. Econ. Geol. 86, 570–587.

Stock, E., Zaki, N., 1972. Antimony dispersion patterns at Costerfield. Min. Geol. J. Vic. 7 (2), 16–22.

Stüwe, K., Keays, R.R., Andrew, A., 1988. Wall rock alteration around gold-quartz reefs at the Wattle Gully mine, Ballarat Slate Belt, central Victoria. In: Goode, A.D.T., Bosma, L.I. (Compilers), Bicentennial Gold '88. Geol. Soc. Aust. Abstr., 22, 478–480.

Sweeney, R.E., Kaplan, I.R., 1973. Pyrite frambiodal formation: Laboratory synthesis and marine sediments. Econ. Geol. 68, 618–634.

Wilkinson, H.E., 1988. Note on the occurrence of thin cone-in-cone limestone beds in the Ordovician turbiditic sediments at Bendigo and Castlemaine. Geol. Surv. Vic. Unpublished Report 51.

Willman, C.E., Wilkinson, H.E., 1992. Bendigo goldfield. Geol. Surv. Vic. Rep. 93, 14–15.